PHOTONIC SENSORS / Vol. 16, No. 1, 2026: 9560005

Frequency-and-Time Division Multiplexed Brillouin Optical Time-Domain Reflectometry

Kezhao GAO, Jianting LI, Yaodong WANG, Shijia ZENG,
Bowen LI*, and Yunjiang RAO*

Key Laboratory of Optical Fiber Sensing & Communications (Ministry of Education of the People's Republic of China), University of Electronic Science and Technology of China, Chengdu 611731, China

*Corresponding authors: Bowen LI and Yunjiang RAO E-mails: bowen.li@uestc.edu.cn and yjrao@uestc.edu.cn

Abstract: Brillouin optical time-domain reflectometry (BOTDR) is a key technique for distributed fiber sensing of strain and temperature, but performance is constrained by the inherently weak spontaneous Brillouin signal. Here, we propose and experimentally demonstrate a novel frequency- and time-division multiplexed BOTDR (FTDM-BOTDR) based on a frequency-stepped light source generated from a frequency-shifting loop. In contrast with existing multi-frequency BOTDR, Brillouin signals from all frequency channels are coherently detected with a single local oscillator (LO) light, maximizing LO power and thus the heterodyne gain for all channels simultaneously. Furthermore, the temporal interleaving of different pump frequencies avoids excessive Kerr nonlinearities. A theoretical model is developed to analyze the signal-to-noise ratio (SNR) in FTDM-BOTDR and illustrate how this single-LO configuration overcomes the SNR limit in conventional multi-frequency BOTDR systems. Using 13 frequency channels, the system achieves the Brillouin frequency shift (BFS) precision of 0.298 MHz at 10 km and a maximum sensing range of 70 km with a 40 ms acquisition time, representing a 3.3-fold precision improvement and a 30 km range extension compared to single-frequency BOTDR. This FTDM-BOTDR technique overcomes key performance bottlenecks of conventional BOTDR and provides a scalable pathway toward high-SNR, long-distance, and real-time distributed temperature or strain sensing.

Keywords: Brillouin scattering; distributed optical fiber sensor; frequency division multiplexing; BOTDR

Citation: Kezhao GAO, Jianting LI, Yaodong WANG, Shijia ZENG, Bowen LI, and Yunjiang RAO, "Frequency-and-Time Division Multiplexed Brillouin Optical Time-Domain Reflectometry," *Photonic Sensors*, 2026, 16(1): 9560005.

1. Introduction

Brillouin scattering-based distributed fiber sensing uniquely measures spatially resolved strain or temperature information based on the dual sensitivity of the Brillouin frequency shift (BFS) to both strain and temperature. Furthermore, owing to its notable advantages including immunity to the electromagnetic interference and long sensing range, this technique has garnered considerable research interests in recent years. Specifically, Brillouin-based fiber-optic sensors can be categorized into those based on stimulated Brillouin scattering (SBS) [1], such as the Brillouin optical time-domain analysis (BOTDA) [2, 3], and those

Received: 17 October 2025 / Revised: 28 December 2025

DOI: 10.26599/PhoS.2026.9560005
Article type: Research article

based on spontaneous Brillouin scattering (SpBS), such as the Brillouin optical time-domain reflectometry (BOTDR) [4, 5]. Among these, the BOTDR offers the unique advantages of single-end access and low system complexity. Requiring access to only one end of the fiber, the BOTDR demonstrates significant operational advantages in scenarios where ease of deployment is a priority. This makes it highly suitable for applications where both ends of the fiber are inaccessible, such as in long-distance pipelines, buried cables, or structural monitoring [6, 7]. Against the backdrop of heightened concerns over the safety and reliability of the critical infrastructure, the BOTDR emerges as an efficacious solution for both structural-health monitoring and temperature monitoring.

However, the scattering efficiency in SpBS is extremely low (−50 dB). In addition, the maximum peak power launched into the fiber is limited by the onset of SBS and modulation instability [8]. As a result, the signal-to-noise ratio (SNR) in the conventional BOTDR system is inherently weak, which directly influences its sensing sensitivity, especially for long-distance sensing. Consequently, long acquisition time for more numbers of averaging is usually required to enhance the detection SNR, prohibiting the application of the BOTDR in scenarios demanding real-time monitoring or rapid response to dynamic changes.

To address this critical challenge, numerous efforts have been made to enhance the SNR of BOTDR systems. For example, distributed Raman amplification [9] has been employed to compensate for the SNR degradation caused by the attenuation of pump energy within the fiber. The use of passive polarization scramblers [10] has also been effective in reducing polarization noise in the system. Additionally, digital signal processing (DSP)-based denoising techniques [11] have been developed to improve the quality of signal processing at the backend.

Beyond these enhancements, innovations at the optical transmitter end has also been shown to be effective, which can be broadly categorized into two types: time-division multiplexing (TDM) and frequency-division multiplexing (FDM). For the TDM, various pulse coding methods [12, 13] have been developed. These methods effectively increase the total input power without raising the peak power, thereby enhancing the system's SNR through the coding gain. On the other hand, the FDM technique utilizes a multi-frequency pump [14] to generate multi-frequency SpBS signals, which are then superimposed to effectively boost the SNR of the BOTDR. Moreover, such enhancement is achieved without increasing the coding length or sacrificing the sensing frame rate.

In the pioneering work conducted by Soto *et al*. [15], a multimode Fabry-Pérot (F-P) laser with the 0.3 nm free spectral range and 10 nm bandwidth was adopted in a BOTDR system, which enhanced the temperature resolution by 4 times to 4 ℃ in the 25 km fiber under test (FUT). Later, a sinusoidal intensity modulated CW light was used as a 10 GHz-spacing three-wavelength source in a BOTDR system, which brought 4.2 dB SNR improvement and a temperature resolution of 0.8 ℃ in the 23.6 km FUT [16]. However, in all the previous works, the multiple pump frequencies were widely spaced, requiring the use of multiple local oscillators (LO) for heterodyne detection. Due to the finite saturation power of the photodetector (PD), the power of each LO was thus limited [17], which inevitably limited the maximum heterodyne gain. Additionally, the multi-frequency pumps were launched simultaneously into the FUT, leading to increased peak power and undesired nonlinear effects [18, 19].

To address the limitations of the FDM based BOTDR discussed above, this study demonstrates a high SNR BOTDR based on the combination of the frequency-and-time-division multiplexing (FTDM), for the first time. Specifically, we have developed a comprehensive theoretical model to analyze the impact of the heterodyne detection gain on the SNR in BOTDR systems. We demonstrate that in the FTDM scheme, employing a single LO signal enables near-saturation power to maximize the heterodyne detection gain across all channels, thereby overcoming the inherent limitations of conventional FDM schemes in optimizing the system SNR. Building on this understanding, we design a frequency-shifting loop to convert a single pulse into a train of pulses with the equal and small frequency increment. Thanks to the small total bandwidth, the Brillouin scattered light generated by all the pump pulses can be heterodyne detected with a single LO, which maximizes the LO power and thus the heterodyne gain for signals in all wavelength channels simultaneously. By averaging the signals from all channels, this scheme effectively improves the SNR, measurement precision, and maximum sensing range without sacrificing the measurement speed. Specifically, using 13 pulses with the 150 MHz frequency spacing, the BFS measurement precision has been improved by 3.3 times compared to the conventional BOTDR, achieving the 0.298 MHz precision in the 11 km FUT using 40 ms acquisition. Furthermore, the maximum sensing distance has been extended from 40 km to 70 km under the criteria of 5 MHz BFS-measurement precision.

Our work introduces a flexible and easily implementable BOTDR scheme based on the FTDM using a frequency-shifting loop. By overcoming the intrinsic limitations of the conventional FDM configuration, the proposed approach achieves notable improvements in the measurement precision and sensing range. Beyond these performance enhancements, the FTDM technique offers high compatibility with other distributed sensing techniques, opening new avenues for scalable, high-precision, and real-time distributed monitoring across long distances.

2. Principle

The basic principle of the FTDM-BOTDR is schematically illustrated in Fig. 1(a). A frequency-shifting loop centered around an acousto-optic modulator (AOM) generates a pulse train with equal frequency increments and time intervals. Due to the small intervals between each frequency channel, a single LO will be used to beat with the Brillouin scattered light from all frequency channels, as shown in Fig. 1(b). The photocurrent for the beat signal between the Brillouin scattered light at the ith frequency and the LO signal is expressed as [20]

$$I_{\text{ph}}^{i}(z) = 2R\sqrt{P_B^{i}(z)P_{\text{LO}}}\cos[(w_1 - w_2^{i})t] \qquad (1)$$

where R is the photodetector responsivity, and P_B^i, w_2^i, P_{LO}, and w_1 are the intensity and frequency of the ith frequency Brillouin scattered light and the intensity and frequency of the LO signal, respectively.

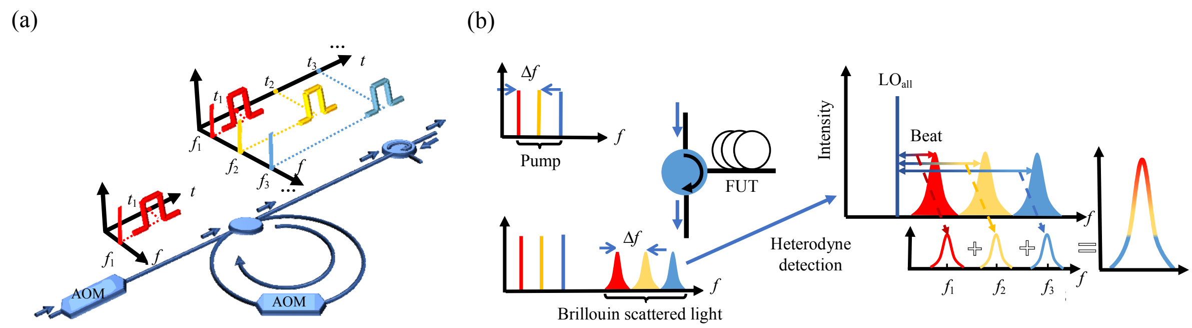

Fig. 1 Working principle of the FTDM-BOTDR: (a) the frequency-shifting loop, centered around the AOM, modulates a single pulse into a pulse train with equal frequency intervals and equal time intervals and (b) schematic of heterodyne detection.

The intensity of Brillouin scattered light at different distances (z) is expressed as $P_B^i(z)=P_B^i(0)e^{-\alpha z}$. So, the SNR of each channel is [21, 22]

$$\mathrm{SNR}_i(z)=\frac{2R^2P_{\mathrm{LO}}P_B^i(z)}{\frac{4kTB_i}{R_L}+2eP_{\mathrm{LO}}B_i+\langle i_n^2\rangle+\langle i_{\mathrm{LO\text{-}ASE}}^2\rangle} \tag{2}$$

where k, T, R_L, e, and B_i are the Boltzmann constant, the PD operating temperature in Kelvin, the load resistance, the elementary charge, and the bandwidth of the ith frequency channel, respectively. The four terms in the denominator represent noises that fall into the bandwidth of each channel, which represent thermal noise and shot noise in the photodetector, the electrical noise from other components such as the oscilloscope, and the beating between the LO and amplified spontaneous emission (ASE), respectively. Since the noise magnitude is the same and uncorrelated for all the N frequency channels, after summation of all channels, the noise increases by $\sqrt{N}$ times, and the signal increases by N times. Therefore, the total SNR will be increased by $\sqrt{N}$ times [23].

$$\mathrm{SNR}(z)=\frac{N\cdot 2R^2P_{\mathrm{LO}}^iP_B^i(z)}{\frac{4kTB}{R_L}+2e\left(\sum_{i=1}^{N}P_{\mathrm{LO}}^i\right)B+\langle i_n^2\rangle+\langle i_{\mathrm{LO\text{-}ASE}}^2\rangle}
=\frac{2R^2P_{\mathrm{LO}}P_B^i(z)}{\frac{4kTB}{R_L}+2eP_{\mathrm{LO}}B+\langle i_n^2\rangle+\langle i_{\mathrm{LO\text{-}ASE}}^2\rangle}. \tag{3}$$

In contrast, for the traditional FDM schemes, the frequency components are widely spaced, and consequently multiple LOs with the same spacing are required. The corresponding heterodyne signals are of the same frequency and directly superimposed in the radio frequency domain. Assuming that the LO power is equal for each channel, the maximum LO power P_{LO}^i is roughly $1/N$ of the PD saturation power P_{LO}, i.e., $P_{\mathrm{LO}}=\sum_{i=1}^{N}P_{\mathrm{LO}}^i=N\cdot P_{\mathrm{LO}}^i$. Therefore, the final SNR by accumulating N channels will remain identical to a conventional single frequency BOTDR, if the maximum LO power is used for both cases.

Therefore, the conventional FDM-BOTDR only exhibits the advantage over the conventional BOTDR when the LO power in the conventional case is far below the saturation power, which however does not represent the operation condition for optimal performance. Therefore, $\sqrt{N}$ times enhancement on the real performance boundary cannot be achieved in principle.

Moreover, according to the SNR model of the BOTDR [24], maximizing LO power enhances the SNR in heterodyne detection. At the fiber far-end, higher LO power drives the detection toward the shot-noise-limited regime and directly improves the SNR. At the near-end, although maximizing LO power offers limited and eventually saturated SNR improvement, it allows lower pulse peak power to be used, thereby suppressing fiber nonlinearities. Hence, operating a single LO near detector saturation simultaneously optimizes noise performance and nonlinear tolerance, which is difficult to achieve in multi-LO FDM-BOTDR systems.

3. Experimental setup

Based on the above principle, the core part of the FTDM-BOTDR system is the frequency-shifting loop, which generates a train of pump pulses with an equal frequency increment and a time interval. As depicted in Fig. 2(a), a single optical pulse enters the loop through a 2×2 fiber optic coupler. One path of the coupler serves as the output of the loop, while the other path is connected to the AOM2 in the loop, which achieves frequency shifting of the pulse. When the frequency-shifted pulses pass through the 2×2 fiber coupler again, 50% is coupled out, while the remaining portion continues to circulate within the loop for subsequent frequency shifting. This process is repeated, thereby modulating a single pulse into a pulse train composed of multiple frequency components. The erbium-doped optical fiber amplifier (EDFA) is responsible for loss compensation. The fiber Bragg grating (FBG) is used to mitigate the degradation of the pulse train's SNR caused by the continuous accumulation of the ASE in the loop. The polarization controller (PC) and the polarization beam splitter (PBS) are employed to maintain a fixed state of polarization in each round trip.

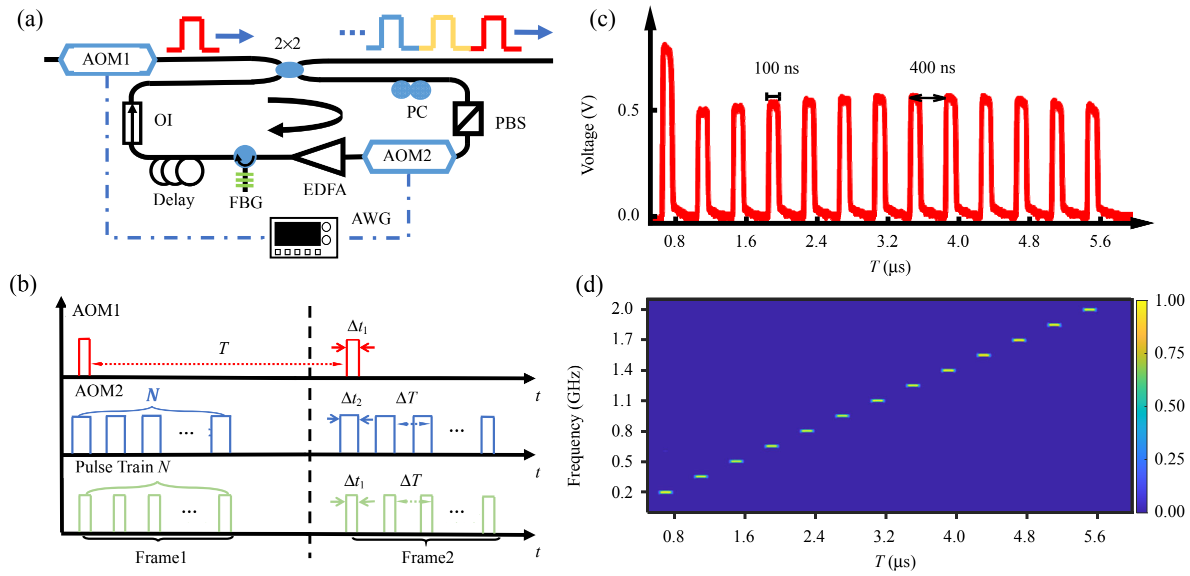

Fig. 2 Setup and characterization of the frequency-shifting loop: (a) setup of the frequency-shifting loop, (b) detailed timing chart of the system (the vertical black dashed lines separate two consecutive frames), (c) time-domain waveform of the pulse train, and (d) frequency-domain curve of the beat-frequency signals generated by the detection pulse train.

To freely control the number of pulses in the pulse train and also prevent self-lasing in the loop, an AOM-control timing sequence shown in Fig. 2(b) is designed [25]. The pulse width Δt_1 and period T controlled by the AOM1 determine the sensing spatial resolution and sensing distance. The gating width of the AOM2 Δt_2 is slightly longer than the pulse width to ensure that the entire pulse is frequency shifted. Its period ΔT corresponds to the loop period, ensuring that the AOM2 is only active and performs pulse frequency shifting when the pulse passes through. When the AOM2 is in the off state, its high insertion loss quickly attenuates the pulses within the loop, thus controlling the total pulse numbers. Through this method, the number of pulses in the pulse train can be customized.

A representative waveform of a pulse train with the 100 ns pulse width and 400 ns interval is shown in Fig. 2(c). By heterodyning the pulse train with a single-frequency laser, the spectrogram of the pulse train is obtained, as shown in Fig. 3(d), clearly presenting the 150 MHz frequency increment and 400 ns delay between each pulse. This temporal interleaving of different frequencies markedly suppresses the peak power, thereby avoiding the onset of excessive Kerr nonlinearities.

The obtained pulse train is then used for the BOTDR, with the experimental setup shown in Fig. 3(a). A narrow-linewidth laser is split into the pump and LO signal through a 50:50 optical coupler. The upper branch is responsible for the generation of the pump. Compared with the conventional FDM-BOTDR, thanks to the small total bandwidth of the pump, the pulse train can be filtered by a single FBG to suppress the ASE from the EDFA1 before entering the FUT, thereby effectively improving the extinction ratio (~45 dB in the current system) and elevating the modulational instability

(MI) threshold. After amplification by the EDFA1, pulses from all channels enter the FUT with roughly equal power, which ensures a quasi-constant SNR among channels, thereby satisfying the prerequisite for the theoretical $\sqrt{N}$ improvement in the SNR. The optical spectrum of the light backscattered from the FUT is shown in the red trace of Fig. 3(b), which is amplified by an EDFA2 (blue trace) and then passed through an FBG2 to significantly attenuate the Rayleigh scattering and the ASE. The final spectrum launched into the balanced photodetector (BPD) is shown by the black trace.

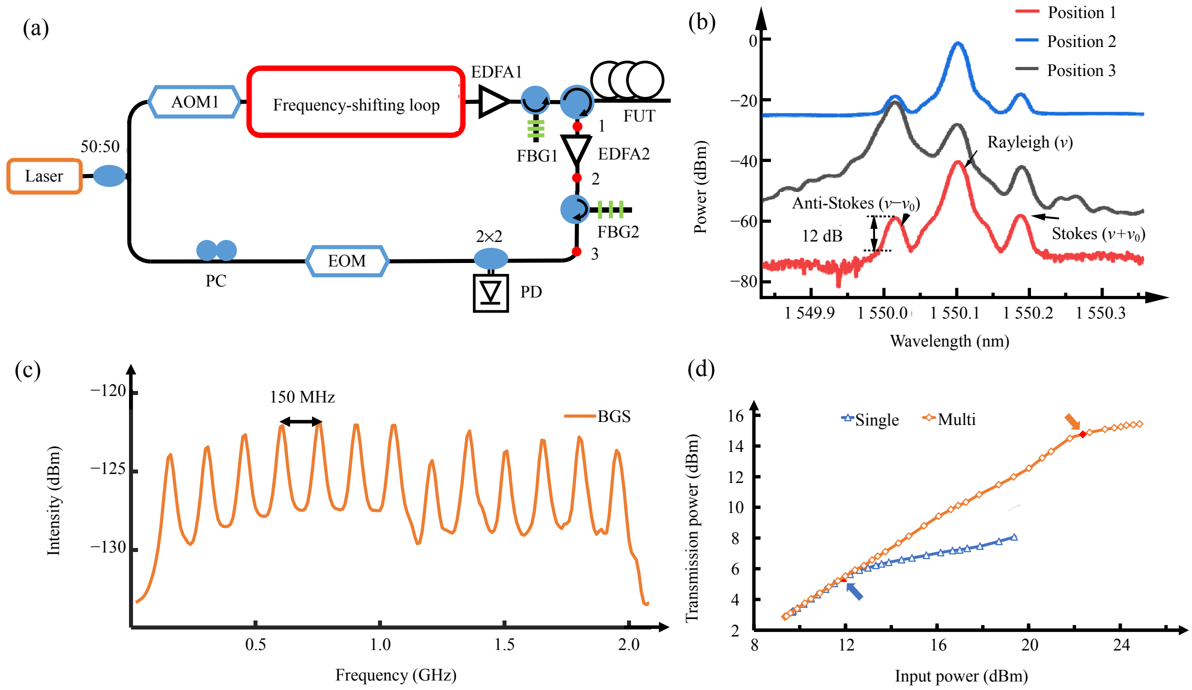

Fig. 3 Experimental setup: (a) setup of the FTDM-BOTDR, (b) optical spectrum of scattered light in different positions, (c) heterodyne detection beat signal, and (d) the Brillouin threshold of the BOTDR in single-frequency and multi-frequency cases.

In the lower branch of the system, the LO is generated by frequency-shifting the narrow-linewidth laser by 10.8 GHz using an electro-optic modulator (EOM), which is then heterodyned with the Brillouin scattered light from all frequency channels simultaneously. Figure 3(c) shows the RF spectrum of the beating signal. The intervals between each Brillouin gain spectrum (BGS) are 150 MHz and the highest frequency in beating signal is 1.95 GHz. The non-uniform intensity of the BGS across different frequencies in Fig. 3(c) primarily arises from the frequency-dependent responsivity of the BPD used in the experiment. Therefore, a 2 GHz-bandwidth BPD is sufficient for heterodyne detection. This single-LO configuration effectively maximizes the LO signal power and thus the SNR during heterodyne detection. Notably, the channel count in this FTDM-BOTDR system is primarily constrained by two aspects: the bandwidth of the BPD and the spacing between frequency components. The high-bandwidth BPDs widely adopted in modern communication systems provide the bandwidth up to 100 GHz, which promises 50 times further scaling for the number of frequency channels without increasing system complexity. The frequency spacing is mainly limited by the BGS width (~50 MHz). Based on the experimental experience, a frequency spacing of at least 100 MHz is recommended when no additional fitting algorithm is employed.

In addition to maximizing the LO power, the multi-frequency nature of this scheme can also increase the maximum input power into the fiber. Since the channel spacing is larger than the Brillouin gain bandwidth, the Brillouin threshold for each channel remains the same as in a single-frequency scenario [26]. Therefore, the Brillouin threshold of the total input power in this scheme is scaled by the pulse number compared to that of a single-frequency pulse. To verify this, we gradually increase the input power by adjusting the EDFA before the FUT and recorded the power changes at the transmission end of the FUT, as shown in Fig. 3(d). The inflection point (arrow) in the curve indicates the onset of the stimulated SBS. The SBS effect transfers most of the pump light energy to the Stokes wave, further increasing the pump light energy loss and causing the transmission end power to plateau. In Fig. 3(d), the power at the inflection point for the multi-frequency case is indeed 13 times higher than that for the single-frequency case.

4. Results

To demonstrate the performance of the FTDM-BOTDR system, the sensing experiment is conducted and compared with the traditional single-frequency BOTDR.

In the experiment, the pulse width is 100 ns, corresponding to the spatial resolution of 10 m and the length of the FUT is 100 km. Figure 4(a) shows the heterodyne beating signal in the FTDM-BOTDR system. In order to obtain BGS information at different positions along the FUT, the short-time Fourier transform (STFT) technique is used [27]. As depicted in Fig. 4(a), the Fourier transform window slides with a step of 100 ns, yielding the BGS at each position along the fiber. The spatial interval between adjacent positions is 10 m, necessitating that the spatial interval matches the spatial resolution to prevent information loss [28]. After the STFT, the BGS spectra of all frequency channels in various time are shown in Fig. 4(b). As observed, the beating signals in different frequency channels have time delays determined by the loop length. Therefore, before cumulatively averaging all channels, delay compensation for each frequency component is required to align different channels temporally. The BGS spectra of all frequency channels, positioned by the OTDR technique, are shown in Fig. 4(c) for various positions in the FUT.

After compensating for the delay, all frequency components are normalized and then averaged. The corresponding result is compared with the single-frequency case, as depicted in Fig. 4(d). For the single-frequency case, the SNR has already deteriorated severely at 40 km, whereas the FTDM-BOTDR still maintains a sufficient SNR at 70 km.

For quantitative characterization, the BFS along the fiber is obtained by Lorentzian fitting using an acquisition time of only 40 ms (~35-period averaging). Figure 5(a) shows how the measurement precision of the single-frequency and FTDM-BOTDR evolves along the fiber. The measurement precision at each spatial location is quantified as the standard deviation calculated from 10 sets of BFS data. After 50 km, the single-frequency BOTDR exhibits Lorentzian-fitting distortion that prevents faithful extraction of the BFS. So, the error grows sharply. With a measurement-precision criterion of 5 MHz, the maximum sensing range for the single-frequency BOTDR is 40 km, while that for the FTDM-BOTDR is substantially extended to 70 km.

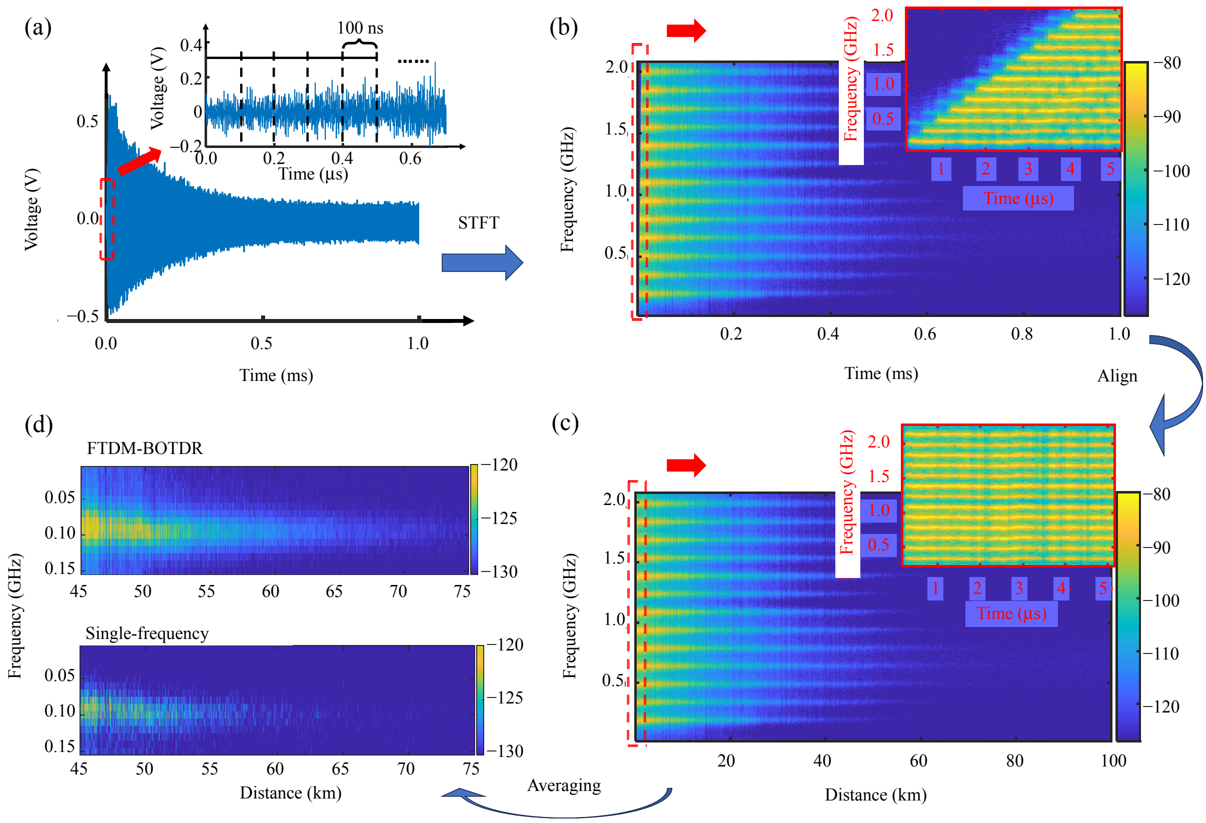

Fig. 4 Data processing of multi-frequency signals: (a) time-domain waveform of the beat signal, (b) BGS at different frequencies after the STFT in various time, (c) BGS at different frequencies at various positions after time-delay compensation, and (d) cumulative averaging of normalized BGS at different frequencies.

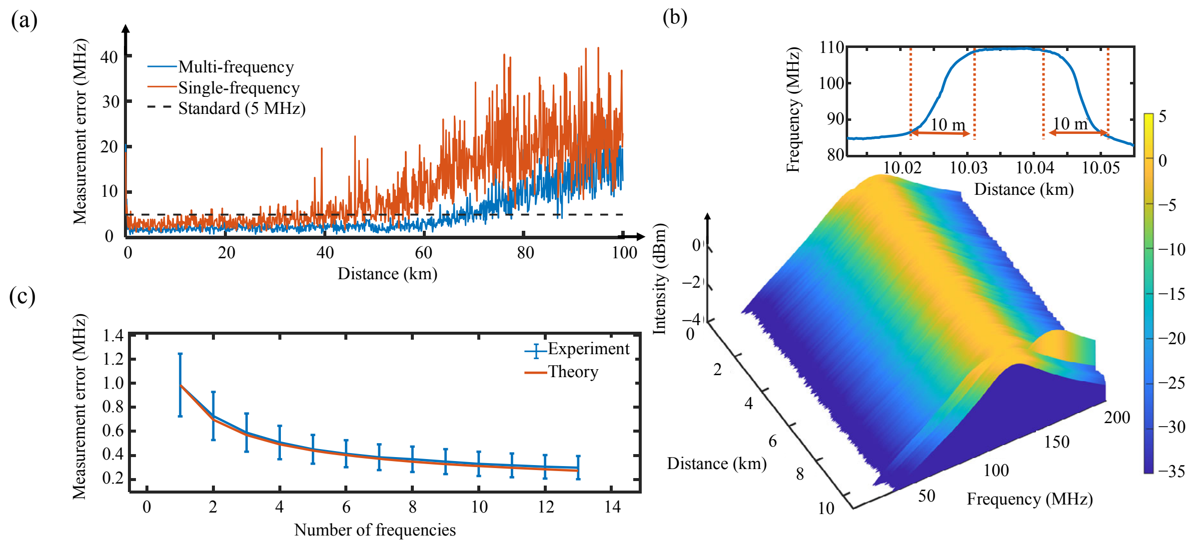

Fig. 5 Experimental results: (a) measurement errors at different positions under long-distance (100 km) conditions, (b) measured 3D spectrum over fiber distance (11 km), and (c) measurement errors with different numbers of averaged frequencies.

In addition, the FTDM-BOTDR also brings the significant enhancement in measurement precision. Figure 5(b) shows the 3-dimensional (3D) view of the BGS distribution curve in a 10 km FUT, whose

20 m section at the end is heated. The inset shows the BFS evolution at the heated section, where the rising and falling edges confirm the 10 m spatial resolution. Figure 5(c) shows the measurement precision at the end of the 10 km FUT using different numbers of pump frequencies with the same acquisition time of 40 ms (~300-period averaging). As the number of frequencies increases, the enhancement of measurement precision evolves with close match to the theoretical value $\sqrt{N}$ (red line). The best measurement precision (N=13) that the current system achieves is 0.298 MHz, representing an enhancement of 3.3 times compared to the single-frequency BOTDR. The discrepancy between the theoretical and experimental SNR improvement (SNRI) is primarily attributed to the influence of the frequency-dependent responsivity of the BPD on the cumulative averaging process. Specifically, because the responsivity of the BPD varies with the frequency, the signal power obtained from each channel during detection is not uniform. This results in an actual increase in the total signal power during cumulative averaging that is lower than the theoretical N-fold improvement, thereby causing the experimentally measured SNRI to be lower than the theoretical $\sqrt{N}$ improvement.

For a better comparison with the FDM-BOTDR, we normalize the measurement precision under different averaging times and define the effective measurement precision without averaging, denoted as $\delta_{\text{eff}} = \delta \times \sqrt{N}$, where δ is the measurement precision obtained after averaging N periods. Table 1 summarizes the normalized error for the FTDM scheme compared with different FDM schemes under varying parameters. The superiority of effective precision in the FTDM-BOTDR is attributed to the larger number of frequency channels and also the higher heterodyne detection SNR enabled by maximizing the LO power.

Table 1 Comparison with the conventional FDM-BOTDR scheme.

Scheme	Averaging periods N	Measurement precision δ	Effective measurement precision δ_{eff}
WDT [28]	2 000	0.47 MHz (at 10 km)	21.02 MHz (at 10 km)
WDT+depolarizer [17]	2 000	0.18 MHz (at 25 km)	8.05 MHz (at 25 km)
WDT+depolarizer+BFL [29]	2 000	0.52 MHz (at 50 km)	23.26 MHz (at 50 km)
FTDM (this work)	35	0.87 MHz (at 10 km) 1.13 MHz (at 25 km) 2.19 MHz (at 50 km)	5.16 MHz (at 10 km) 6.71 MHz (at 25 km) 12.96 MHz (at 50 km)

To further highlight the role of the TDM characteristic and single-LO heterodyne detection in the FTDM-BOTDR, it is worthwhile to discuss the performance difference between the FTDM and conventional FDM with the same number of frequency components. Compared with a conventional FDM scheme [29] and under the same sensing distance (~10 km) without using a depolarizer, the FTDM-BOTDR with only three frequency components achieves a measurement error of 0.57 MHz (~300-period averaging) and an effective error of 9.87 MHz, which is still lower than the 21.02 MHz reported for the WDT scheme [29]. This result suggests that the SNR improvement of the FTDM-BOTDR is not only due to an increased number of frequency components, but also benefits from its TDM operation and the use of a single LO to maximize the heterodyne gain for all channels.

The experimental results are obtained under practical hardware constraints in data acquisition. Owing to the frequency-division multiplexing scheme, the FTDM-BOTDR system requires a wide acquisition bandwidth and a high sampling rate. Under long-distance sensing conditions (~100 km), the limited memory depth of the data acquisition unit allows at most 35 periods to be recorded in a single acquisition. Although multiple acquisitions could be combined to increase the effective averaging, the accurate temporal alignment between acquisitions is required, and any misalignment would affect the measured performance.

5. Discussion

The FTDM architecture proposed exhibits strong compatibility with other BOTDR SNR enhancing techniques. For pulse coding, the attainable coding length per channel is dictated by the pulse width of each bit and the loop period. For example, by slightly increasing the loop period to 1 280 ns and adopting a 10 ns pulse width, a 128-bit code can be assigned to every channel. In this way, the meter-level spatial resolution could be realized along with the high SNR. Moreover, the FTDM scheme can also be seamlessly integrated with distributed Raman amplification, which can extend the sensing distance and boost the signal strength for all frequency channels simultaneously, thereby comprehensively improving overall sensing performances of the BOTDR.

Although the proposed FTDM-BOTDR system demonstrates clear advantages in terms of the sensing range, measurement precision, and nonlinear suppression, its dynamic range is inherently constrained by the frequency spacing between adjacent channels. In the present implementation, the BGS of neighboring channels is separated by 150 MHz. When fiber perturbations induce a Brillouin frequency shift exceeding this spacing, the relative time delay among different channels leads to the spectral overlap after the STFT processing, resulting in BGS aliasing and inaccurate BFS extraction. This limitation reflects a fundamental trade-off in FTDM-BOTDR systems between the number of frequency channels and the achievable dynamic range, and should be considered in the system design depending on the expected magnitude of environmental perturbations.

In summary, we have proposed and demonstrated a frequency-and-time-domain multiplexed BOTDR system based on a frequency-shifting loop. It not only obtains multiple sensing signals parallelly through frequency multiplexing, but maximizes the LO power for heterodyne detection, thus significantly improving the detection SNR. Meanwhile, because the FDM scheme accumulates and averages the different frequency channels, intrinsically reducing the volume of raw data required for averaging, we can shorten the acquisition time and expand the system's measurement bandwidth. Additionally, the time-domain interleaving configuration simultaneously avoids the excessive peak power and suppresses fiber nonlinearities that are inevitable in the existing FDM BOTDR. Compared to the single-frequency BOTDR, this work achieves the high measurement precision of 0.298 MHz at 10 km and a long sensing range of 70 km with 4.882 MHz precision within a very short measurement time of 40 ms. In the current era, when the requirement for the sensing range and precision is perpetually increasing, this FTDM-BOTDR technology establishes a promising solution for long-range and high-precision temperature or strain sensing in a real-time manner.

Acknowledgment

This work is supported by the Key Program of the Natural Science Foundation of China (Grant No. U21A20453) and the General Program of Natural Science Foundation of China (Grant No. 62575053).

Declarations

Conflict of Interest Yunjiang RAO is the editor-in-chief and was not involved in the editorial review, or the decision to publish this article. All authors declare that there are no competing interests.

Use of AI Statement None.

References

[1] M. Merklein, I. V. Kabakova, A. Zarifi, and B. J. Eggleton, “100 years of Brillouin scattering: historical and future perspectives,” *Applied Physics Reviews*, 2022, 9(4): 041306.
[2] T. Horiguchi, T. Kurashima, and M. Tateda, “A technique to measure distributed strain in optical fibers,” *IEEE Photonics Technology Letters*, 1990, 2(5): 352–354.
[3] Y. Dong, “High-performance distributed Brillouin optical fiber sensing,” *Photonic Sensors*, 2021, 11(1): 69–90.
[4] T. Kurashima, T. Horiguchi, H. Izumita, S. Furukawa, and Y. Koyamada, “Brillouin optical-fiber time domain reflectometry,” *IEICE Transactions on Communications*, 1993, 76(4): 382–390.
[5] Q. Bai, Q. Wang, D. Wang, Y. Wang, Y. Gao, H. Zhang, *et al*., “Recent advances in Brillouin optical time domain reflectometry,” *Sensors*, 2019, 19(8): 1862.
[6] H. F. Pei, J. Teng, J. H. Yin, and R. Chen, “A review of previous studies on the applications of optical fiber sensors in geotechnical health monitoring,” *Measurement*, 2014, 58: 207–214.
[7] C. Y. Hong, Y. F. Zhang, G. W. Li, M. X. Zhang, and Z. X. Liu, “Recent progress of using Brillouin distributed fiber optic sensors for geotechnical health monitoring,” *Sensors and Actuators A: Physical*, 2017, 258: 131–145.
[8] M. Alem, M. A. Soto, and L. Thévenaz, “Analytical model and experimental verification of the critical power for modulation instability in optical fibers,” *Optics Express*, 2015, 23(23): 29514.
[9] Y. T. Cho, M. Alahbabi, M. J. Gunning, and T. P. Newson, “50-km single-ended spontaneous-Brillouin-based distributed-temperature sensor exploiting pulsed Raman amplification,” *Optics Letters*, 2003, 28(18): 1651.
[10] F. Wang, C. Li, X. Zhao, and X. Zhang, “Using a Mach-Zehnder-interference-based passive configuration to eliminate the polarization noise in Brillouin optical time domain reflectometry,” *Applied Optics*, 2012, 51(2): 176.
[11] W. Yang, Y. Yang, and M. Yang, “Fast digital envelope detector based on generalized harmonic wavelet transform for BOTDR performance improvement,” *Measurement Science and Technology*, 2014, 25(6): 065103.
[12] Y. Q. Hao, Q. Ye, Z. Q. Pan, H. W. Cai, and R. H. Qu, “Digital coherent detection research on Brillouin optical time domain reflectometry with simplex pulse codes,” *Chinese Physics B*, 2014, 23(11): 110703.
[13] S. Wan, Y. Xiong, and X. He, “The theoretical analysis and design of coding BOTDR system with APD detector,” *IEEE Sensors Journal*, 2014, 14(8): 2626–2632.
[14] J. T. Li, B. Chang, J. T. Du, T. Tan, Y. Geng, H. Zhou, *et al.*, “Coherently parallel fiber-optic distributed acoustic sensing using dual Kerr soliton microcombs,” *Science Advances*, 2024, 10(3): eadf8666.
[15] M. A. Soto, G. Bolognini, and F. D. Pasquale, “Distributed optical fibre sensors based on spontaneous Brillouin scattering employing multimode Fabry-Pérot lasers,” *Electronics Letters*, 2009, 45(21): 1071–1072.
[16] C. Li, Y. Lu, X. Zhang, and F. Wang, “SNR enhancement in Brillouin optical time domain reflectometer using multi-wavelength coherent detection,” *Electronics Letters*, 2012, 48(18): 1139–1141.
[17] N. Lalam, W. P. Ng, X. Dai, Q. Wu, and Y. Q. Fu, “Performance analysis of Brillouin optical time domain reflectometry (BOTDR) employing wavelength diversity and passive depolarizer techniques,” *Measurement Science and Technology*, 2018, 29(2): 025101.
[18] T. Horiguchi, K. Shimizu, T. Kurashima, M. Tateda, and Y. Koyamada, “Development of a distributed sensing technique using Brillouin scattering,” *Journal of Lightwave Technology*, 1995, 13(7): 1296–1302.
[19] Z. Zhang, Y. Lu, and Y. Zhao, “Channel capacity of wavelength division multiplexing-based Brillouin optical time domain sensors,” *IEEE Photonics Journal*, 2018, 10(1): 1–15.
[20] Y. Li, X. Li, Q. An, and L. Zhang, “Detrimental effect elimination of laser frequency instability in Brillouin optical time domain reflectometer by using self-heterodyne detection,” *Sensors*, 2017, 17(3): 634.
[21] A. Zornoza, M. Sagues, and A. Loayssa, “Self-heterodyne detection for SNR improvement and distributed phase-shift measurements in BOTDA,” *Journal of Lightwave Technology*, 2012, 30(8): 1066–1072.
[22] M. A. Soto, and L. Thévenaz, “Modeling and evaluating the performance of Brillouin distributed optical fiber sensors,” *Optics Express*, 2013, 21(25): 31347.
[23] J. Hu, B. Chen, G. Li, and Z. Lin, “Methods for signal-to-noise ratio improvement on the measurement of temperature using BOTDR sensor,” in *Advanced Sensor Systems and Applications IV*, Beijing, China, Nov. 9, 2010, pp. 59–65.

[24] S. Jin, Z. Yang, X. Hong, and J. Wu, "Analytical signal-to-noise ratio model on frequency-scanned Brillouin optical time-domain reflectometry," *Journal of Lightwave Technology*, 2024, 42(16): 5786–5796.
[25] B. Li, S. W. Huang, Y. Li, C. W. Wong, and K. K. Y. Wong, "Panoramic-reconstruction temporal imaging for seamless measurements of slowly-evolved femtosecond pulse dynamics," *Nature Communications*, 2017, 8(1): 61.
[26] Y. Aoki and K. Tajima, "Stimulated Brillouin scattering in a long single-mode fiber excited with a multimode pump laser," *Journal of the Optical Society of America B*, 1988, 5(2): 358.
[27] J. Geng, S. Staines, M. Blake, and S. Jiang, "Distributed fiber temperature and strain sensor using coherent radio-frequency detection of spontaneous Brillouin scattering," *Applied Optics*, 2007, 46(23): 5928.
[28] F. Wang, X. Zhang, Y. Lu, R. Dou, and X. Bao, "Spatial resolution analysis for discrete Fourier transform-based Brillouin optical time domain reflectometry," *Measurement Science and Technology*, 2009, 20(2): 025202.
[29] N. Lalam, W. P. Ng, X. Dai, Q. Wu, and Y. Q. Fu, "Performance improvement of BOTDR system using wavelength diversity technique," in *2017 25th Optical Fiber Sensors Conference*, Jeju, South Korea, Apr. 24–28, 2017, pp. 1–4.
[30] N. Lalam, W. P. Ng, X. Dai, Q. Wu, and Y. Q. Fu, "Performance improvement of Brillouin ring laser based BOTDR system employing a wavelength diversity technique," *Journal of Lightwave Technology*, 2018, 36(4): 1084–1090.